

MAVIS Adaptive Optics Module Optical Design

Davide Greggio^{*a}, Demetrio Magrin^a, Christian Schwab^b, Simone Di Filippo^{a, c}, Valentina Viotto^a, Maria Bergomi^a, Enrico Pinna^d, Marco Bonaglia^d, Guido Agapito^d, Thierry Fusco^e, Benoit Neichel^e, François Rigaut^f, Stefan Ströbele^g, Matteo Aliverti^h, Bernard Delabreⁱ, Nicholas Herral^f, Kalyan Radhakrishnan^a, Luca Marafatto^a

^a INAF – Osservatorio Astronomico di Padova, Vicolo dell'Osservatorio 5, 35122 Padova, Italy

^b Australian Astronomical Optics – Macquarie University, 105 Delhi Rd, North Ryde NSW, 2113

^c Dipartimento di Fisica ed Astronomia G. Galilei – Università degli Studi di Padova, Vicolo dell'Osservatorio, 3, 35122 -Padova, Italy

^d INAF – Osservatorio Astrofisico di Arcetri, Largo Enrico Fermi, 5, 50125 Firenze, Italy

^e Laboratoire D'astrophysique De Marseille, 38 Rue Frédéric Joliot Curie, 13013 Marseille, France

^f The Australian National University, Mount Stromlo Observatory Weston ACT 2611

^g European Southern Observatory, Karl-Schwarzschild-Straße 2, 85748 Garching, Germany

^h INAF-Osservatorio Astronomico di Brera, Via E. Bianchi, 46, 23807 San Rocco LC, Italy

ⁱ Bernard Delabre consulting

ABSTRACT

The MCAO Assisted Visible Imager and Spectrograph (MAVIS)^[1], is a new instrument for ESO's Very Large Telescope. The instrument will be installed at the Nasmyth focus of the UT4 telescope and is comprised of an imager and a spectrograph which will take advantage of the unprecedented angular resolution and sky coverage provided by LGS assisted MCAO correction at visible wavelengths. The Adaptive Optics Module (AOM) is the core engine of MAVIS, devoted to multi-conjugate wavefront sensing and correction, and designed to deliver a 30x30 arcsec² corrected field of view to the scientific instruments.

In this paper we focus on the optical design of the AOM, which has been optimized to perform several tasks including field de-rotation, atmospheric dispersion correction, and adaptive optics closed-loop operations. To maximize sky coverage, the system is designed to deliver a 2 arcmin field of view for the selection of up to 3 NGS for measurement of tip-tilt. The AOM module also includes a multiple LGS WFS for high-order wavefront measurements and two post-focal DMs for wide field turbulence compensation.

The proposed design is the result of a trade-off study in which particular care has been devoted to satisfy performance and operational requirements, as well as modularity. We present here a complete description of the selected optical configuration with a summary of the performance analyses.

Keywords: MAVIS, optical relay, adaptive optics, adaptive optics module, MCAO, performance analysis, optical design

1. INTRODUCTION

The Adaptive Optics Module (AOM) of MAVIS is a self-contained MCAO module able to deliver an AO-corrected field of view of 30x30 arcsec to the instruments and providing at least two output ports. The instruments currently foreseen in MAVIS are an imager^[2] with a 7mas/pixel scale that will observe at visible wavelengths (370-1000nm) and that will be equipped with several broad and narrow band filters, and an IFU spectrograph^[2] which is characterized by a high-resolution mode (3"x3", R~12000), and a low resolution mode (6"x6", R~5000). MAVIS recently underwent its Phase A study during which several design options were envisaged^[3]. In this paper we provide a detailed description of the selected baseline design for the AOM. We start by giving a summary of the requirements driving the design, then we describe the selected configuration and finally, we present the estimated performances of the system.

*davide.greggio@inaf.it;

2. DESIGN REQUIREMENTS

MAVIS will be installed at the VLT UT4 and, as such, it will use the already existing Adaptive Optics Facility (AOF, [4]) composed by a deformable secondary mirror (DSM) with 1170 actuators and 4 Laser Guide Stars (LGS). The requirement in terms of atmospheric turbulence compensation is to achieve a Strehl Ratio (SR) of:

- $SR \geq 10\%$ (goal 15%) for $m_J \approx 8$ TT-stars (class G2);
- $SR \geq 7\%$ for $m_J \approx 15$ (TBC) TT-stars (class G2).

Considering Sky Coverage, it is required a correction of $SR \geq 7\%$ (average) in V-band in standard atmospheric conditions in at least 50% of the pointings at the Galactic pole.

This requirement is very demanding since it translates into a residual wavefront error $< 130\text{nm}$, including AO related errors (fitting error, tomographic error, temporal error, aliasing, etc...), NCPA aberrations and manufacturing and alignment tolerances (see [5]). To achieve this level of correction it is necessary to keep the errors due to manufacturing and alignment below $\sim 10\text{-}20\text{nm}$ RMS WFE

Concerning the output of the AOM, the top-level requirements (TLRs) call for a 30arcsec corrected FoV with minimal distortion, optimized in the visible (VRI), but with the goal to preserve also the UBz part of the spectrum as available for the post focal instrumentation. This means that a certain level of correction and throughput is required down to 370nm, setting constraints for what concerns chromatic aberrations and selection of UV-transparent glasses.

Finally, the system is required to be modular in order to ease interactions within the consortium and mitigate risks and costs during the design and AIV phases.

3. AOM DESIGN DESCRIPTION

The baseline AOM optical design selected for phase A is the result of a trade-off study that involved the comparison of all-reflective, all-refractive and catadioptric solutions^[3]. The selected configuration presented below is the all-refractive one.

The modular approach is reflected in the basic architecture of the AOM as well (see Figure 1), which is composed by three main sub-modules:

- *Post focal relay optics (PFR)*: it collects the light from the UT4 Nasmyth focal plane and relays it to the instruments and the other sub-modules. It includes a common path, in which the meta-pupils are re-imaged onto two post-focal DMs, located at 6km and 13.5km. The LGS light (589nm wavelength), devoted to high order modes retrieval, is then split by means of a dichroic reflecting the laser light to the LGS channel and transmitting the NIR and VIS light. The common path between NIR and VIS light includes a wide band common ADC and an optical de-rotator to compensate for the apparent rotation of the sky. Then, the light is split into the Science channel (visible light in the 370-1000 nm band) and the NGS WFS channel (NIR light in the 1000-1700 nm band, even if an extension to 1800 nm is being considered), devoted to low order modes sensing. The PFR also serves as input interface for the calibration unit (CU).
- *LGS wavefront sensor (LGS-WFS)*: The High Order (HO) wavefront sensor of MAVIS. The current baseline calls for 8 LGSs with a circular asterism. The LGS WFS includes means for de-rotation of its FoV to compensate for change in the telescope elevation.
- *NGS wavefront sensor (NGS-WFS)*: The Low Order (LO) wavefront sensor of MAVIS. The current baseline enables 3 NGSs to be sensed, in the J+H bands, at the same time, in a 2 arcmin diameter unobstructed FoV.

The configuration, position of optical elements along the optical train, number of wavefront sensors and, more generally, many of the optical specifications are the result of other trade-off studies that were conducted at system level^[5]. The most relevant ones are summarized in Table 1 and detailed in the design description.

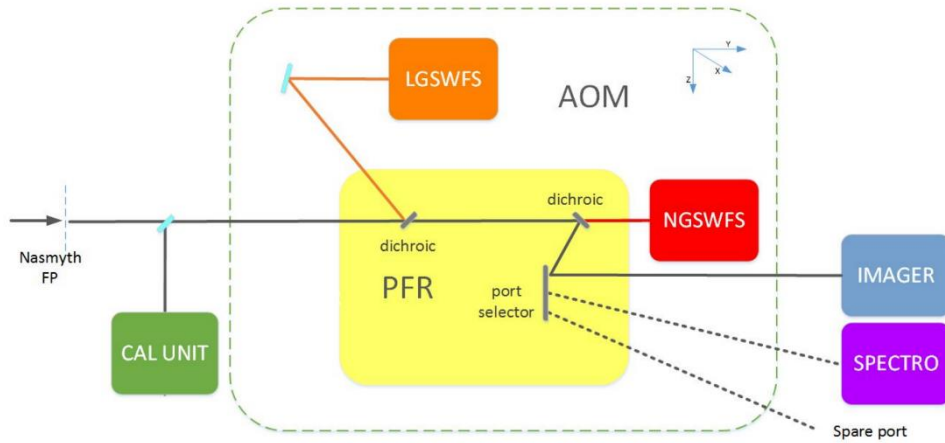


Figure 1. Illustration of the main modules and sub-modules of MAVIS.

Table 1. AOM optical requirements and assumptions

GENERAL	
De-rotation scheme	Common optical derotation for science instruments and NGS WFSs Mechanical derotation for LGS sub-module
Atmospheric dispersion compensation	Broadband atmospheric dispersion corrector in NGS+Science common path
DEFORMABLE MIRRORS	
DM_High conjugation height [km]	13.5
DM_Low conjugation height [km]	6
DM_High projected pitch [cm]	32
DM_Low projected pitch [cm]	25
NGS SUB-MODULE	
Field of view radius [arcsec]	60
Waveband [nm]	1000-1700
Telecentricity	Telecentric (req. TBD)
Number of NGSs	3 stars anywhere within the FoV
LGS SUB-MODULE	
Field of view radius [arcsec]	17.5
Conjugation distance [km]	80-230
Telecentricity	Telecentric (req. TBD)
Number of LGSs, asterism	8, circular asterism
SCIENCE INSTRUMENTS	
Field of view [arcsec]	30x30
Waveband [nm]	370-1000
Telecentricity	<1°
Plate scale to instruments	0.74 arcsec/mm (avoid re-imaging optics for the imager)

3.1 Post-focal relay optics

The PFR optical design is composed by on-axis refractive elements. This configuration has the advantage of being more versatile with respect to off-axis mirrors designs in which geometrical symmetry is usually required to control aberrations and distortion. The main disadvantage is the presence of chromatic aberrations that need to be carefully controlled by a proper choice of glasses.

The layout of the optical design of the PFR is shown in Figure 2. The first element is a field lens, which is kept at >500mm distance from the Nasmyth adaptor/rotator flange to avoid the need to move part or the whole AOM during maintenance activities. The field lens will be used as a compensator for pupil shift.

The field lens acts at the same time as window of the MAVIS enclosure and as imaging optics generating a high-quality image of the meta-pupils at 6km and 13.5km altitude onto the DMs. Just before the DMs, a flat folding mirror can be inserted in the beam to inject the light from the calibration unit inside MAVIS while, after the DMs, a collimating doublet forms an accessible image of the telescope pupil at a distance of 55mm from its last surface. In the collimated beam are also placed:

- the Na dichroic, reflecting the LGS light at 589nm to the LGS re-imaging optics;
- the Atmospheric Dispersion Corrector (ADC), providing optimized atmospheric dispersion compensation from 450 to 1700nm and consisting of two counter-rotating prisms (see [6]);
- the K-mirror for sky de-rotation;
- the VIS/NIR dichroic transmitting the NIR light to the NGS re-imaging optics and reflecting the VIS light to the Science channel.

A 3-lens objective on the NGS channel generates an F/20.6 telecentric and flat focal plane for the NGS WFS sub-module. The LGS WFS entrance focal plane is F/8.9 and is kept fixed thanks to a focusing mechanism (the LGS range compensation mechanism), composed by a triplet with two elements moving together, which allows refocusing of the LGS images, when the Sodium layer moves within the 80km-230km range. The focusing at different ranges is achieved by moving a translation stage along the optical axis, similar to the implementation in GALACSI^[7].

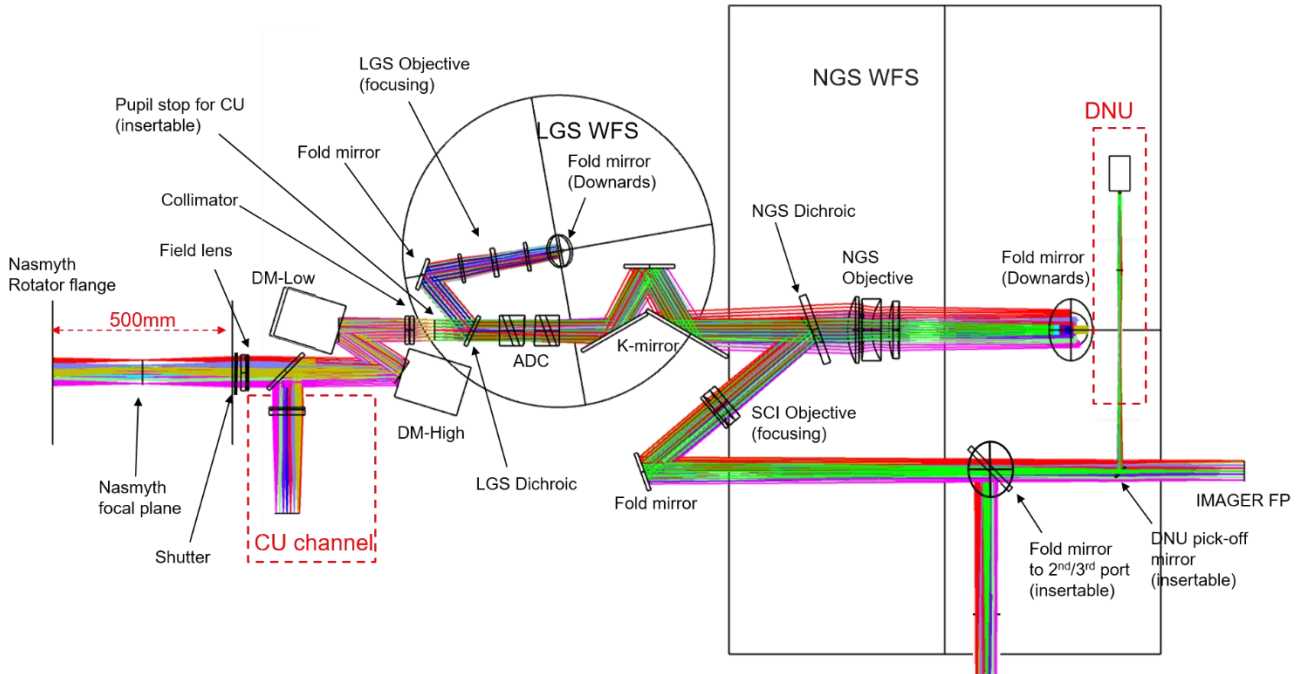


Figure 2. Optical layout of the AOM Post Focal Relay (top view of the optical bench)

In the science channel, the visible light is focused by a 3-lens objective delivering an F/35 (plate scale 0.74 arcsec/mm) beam with long focal extraction. The objective is mounted on a linear translation stage to allow refocusing between the NGS WFS and the instrument. The beam is directed towards the Imager by a flat folding mirror, while another dedicated flat mirror can be inserted to direct the light towards the Spectrograph. An additional folding mirror can finally direct the light towards the DNU (Diagnostics and NCPA Unit), which is a camera characterized by a smaller FoV, used for NCPA calibrations and offline diagnostics.

3.2 Natural Guide Star WFS sub-module

The current design for the NGS WFS sub-module includes the three NGS WFSs and one acquisition camera. Each WFS is fed with light from one natural guide source, selected from the unobstructed technical field of 120 arcsec diameter transmitted by the NGS dichroic ($\lambda > 1\mu\text{m}$) and focused on a f/20.6 beam by the NGS objective. The system is designed such that each WFS can move over the whole FoV in order to maximize the sky coverage.

The NGS WFSs are in charge of providing both atmospheric tip-tilt estimation and truth sensing measurement. The adopted solution foresees 3 WFSs with 2x2 sub-apertures fed by the J-H flux of 1 NGS each, providing both tip-tilt and low order truth sensing for each NGS. In case of faint NGSs the corresponding sensor can be switched to a 1x1 configuration, limiting its functionality to tip-tilt measurement only, but maximizing sensitivity and sky coverage.

An overall view of the entire NGS WFS sub-module is given in Figure 3. The optical path from the PFR is folded downward by a fold mirror (not in figure) ~575mm before the exit focal plane of the relay. Each of the 3 NGS WFS is mounted on a pair of orthogonal linear stages (“XY” stages) with 100x100mm travel range. The linear stages are mounted on slightly different levels, along the optical axis, to avoid collisions between them. An Acquisition Camera is positioned below the 3 NGS WFS, fed by the direct NGS focal plane. This device is able to re-image the full NGS technical FoV on a InGaAs detector.

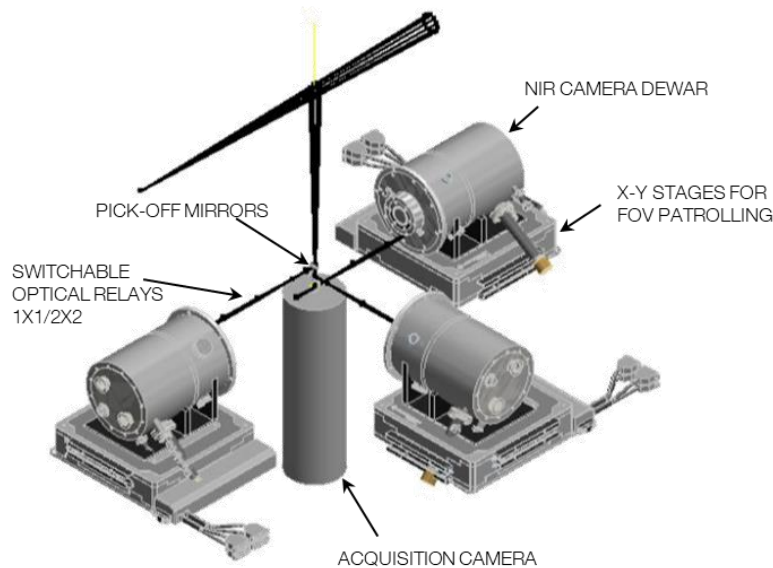


Figure 3. 3D model of the NGS WFS sub-module

The internal configuration of an NGS WFS is shown in Figure 4. The first optical element of each WFS is a pick-off mirror (POM) at 45° angle of incidence. The obstruction caused by the POM is equivalent to ~6 arcsec projected on the focal plane. To reduce contamination from neighboring stars in crowded fields and minimize the NIR sky background, a field stop equivalent to 4 arcsec diameter on-sky is implemented on each probe, located after the POM in correspondence of the F/20.6 focal plane delivered by the PFR.

The 1x1 scheme implements a 3f design, in which 2 lenses produce a 1:1 optical relay, maintaining the F/20.6 focal ratio, corresponding to the scale of 30 mas/pixel onto the SAPHIRA detector^[8]. In the 2x2 scheme, instead, the last focusing lens is replaced with a 2x2 lenslet array whose focal length is selected to have a diffraction limited PSF sampled with 2 pixels.

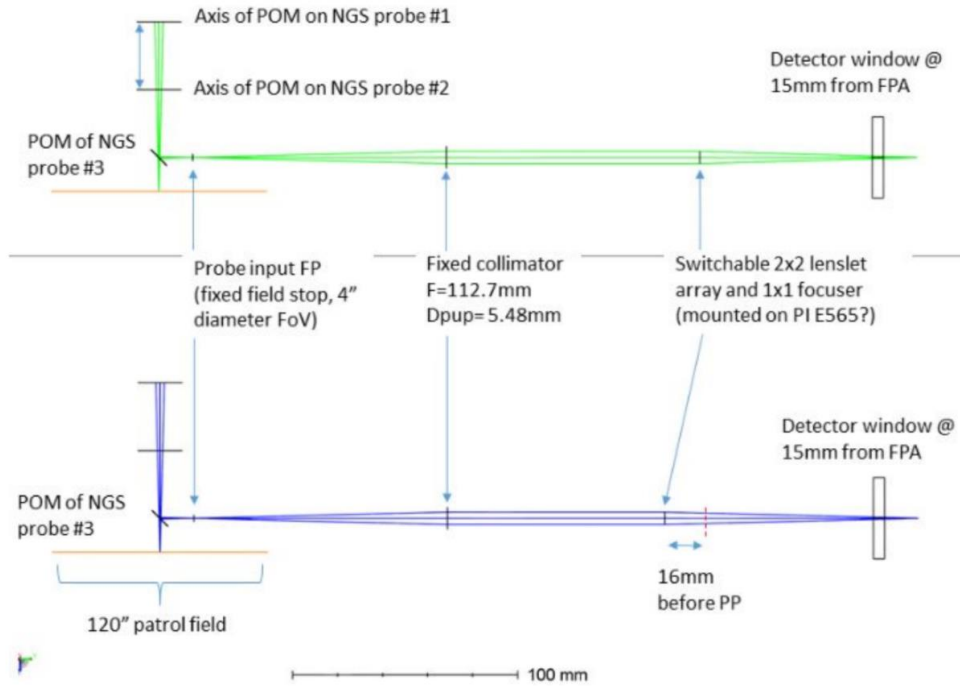


Figure 4. The 2x2 (green, top) and 1x1 (blue, bottom) layout of the optical relays in the NGS WFS. The first elements (POM, field stop and collimator) are in common path between the two, while a linear stage allows to switch between a focuser or 2x2 lenslet to implement the different pupil sampling layouts.

The acquisition camera, positioned below the NGS WFSs., is able to image the full patrol FoV onto an InGaAs sensor. As a baseline, we consider the First Light C-RED2 detector^[9], having $QE \approx 90\%$ (at -40°C) in the wavelength range 0.95-1.6 μm on a frame 640x512 pixels with 15 μm side. A 12.5x optical demagnification will fit the full 120" patrol field on the camera frame. A possible layout for a suitable objective, based on refractive elements, is shown in Figure 5. The 96 mm diameter input FoV is compressed by 12.5 times by a refractive objective composed by three lenses. The total length from the input F/20.6 focal plane to the output F/1.65 focal plane is approximately 300mm. The telescope PSF is fully imaged on a 4x4 pixel area, but 50% of the energy is enclosed in a 2x2 pixel area.

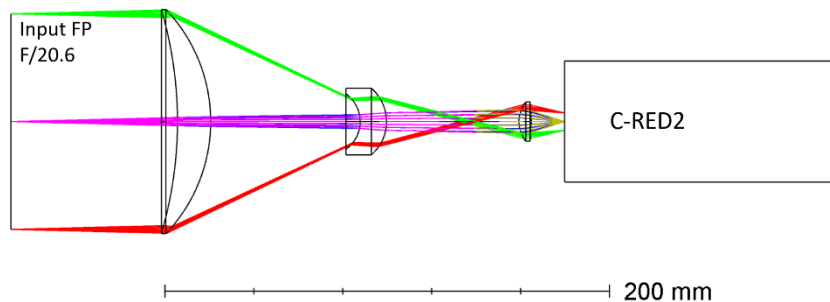


Figure 5. Optical layout of the acquisition camera based on a First Light C-RED2 detector.

3.3 Laser Guide Star WFS sub-module

The Laser Guide Star WFS sub-module is used to measure high-order modes. Based on the results of the numerical analysis^[10], the current MAVIS baseline design makes use of eight LGs fixed at a radius of 17.5". The eight LGs are

produced by splitting in two parts the light from each of the four laser launch telescopes already part of the AOF. The LGS WFS sub-module therefore incorporates eight WFSs and the associated support equipment. One important aspect of the design (de-rotation scheme + on-axis PFR optics) is that the nominal NCPAs are rotationally symmetric, so that NCPA should not depend on the clocking angle of the LGS constellation. This is fundamental for the good control of the NCPAs, for which the allocated error budget is only 25nm.

Figure 6 shows the optical design of the WFS sub-module. The WFS receives a F/8.9 focal plane in which the focal plane position, the plate scale and the exit pupil are stabilized by the PFR to compensate for the change in the distance of the LGS sources, due to UT4 elevation. Close to that focal plane, an eight-faced reflective pyramid splits the light coming from the different LGSs into their respective WFS arm. Each WFS arm consists of a collimator, an image steering mirror, another relay with a field stop, the lenslet array and the focal plane. The image steering mirrors redirect the beam down to the camera and are acting as compensators for differential movements between LGSs images produced from a single laser launcher.

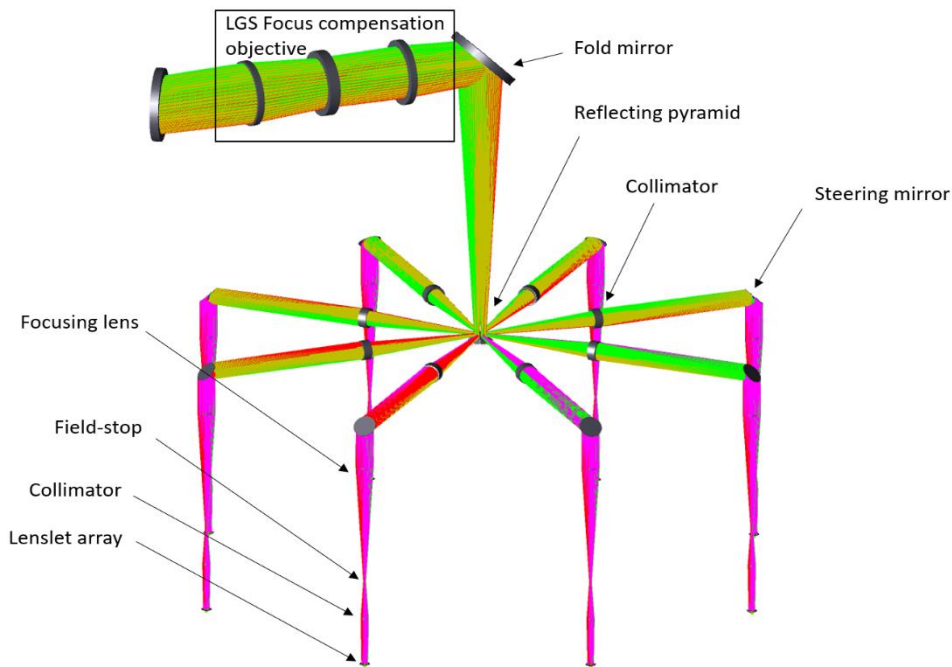


Figure 6. A shaded layout of the LGS WFS Design. The LGS focus compensation mechanism lenses, part of the PFR, are shown for reference.

Each LGS WFS maps a 5" FOV onto a 6x6 pixel spot with a 40x40 sample of the exit pupil on the CCD220. The CCD220 has 24µm square pixels so the size of the exit pupil must be 5.760 mm to completely fill the CCD with spots of 6 square pixels.

4. AOM OPTICAL PERFORMANCE

4.1 Post-focal relay optics

The optical quality of the PFR has been optimized in terms of residual RMS wavefront error. Figure 7 shows the nominal RMS WFE expressed in waves as a function of wavelength for different positions across the science channel FoV (denoted by different colors). The design is diffraction limited from 400nm up to 1000nm. The worse optical quality below 400nm

is due to the reduced weight assigned to that part of the spectrum. This is justified by the lower level of correction delivered by the AO at short wavelengths.

As shown in Figure 8 and Figure 9, the image quality is diffraction limited also at the LGS and NGS focal planes produced by the PFR and that serve as interface for the WFS sub-modules. Note that, in the case of the LGS focal plane (Figure 9), we show the RMS WFE as a function of FoV, and colors denote different conjugation distances.

Finally, the image quality of the meta-pupils formed on the DMs has been evaluated in terms of geometric ensquared energy, with more than 98% of the energy enclosed within a square having side $1/10^{\text{th}}$ of the DM actuator size for both the low and high-altitude layers.

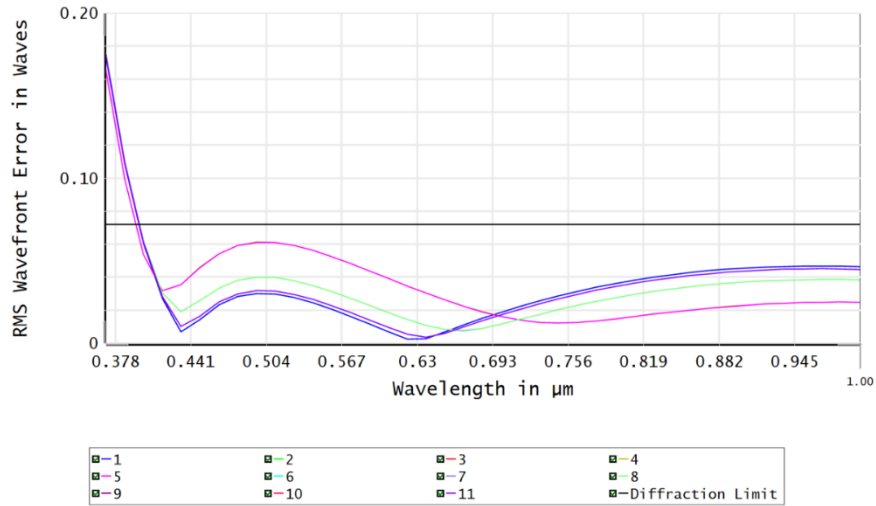


Figure 7. Nominal WFE RMS vs. wavelength in the science channel

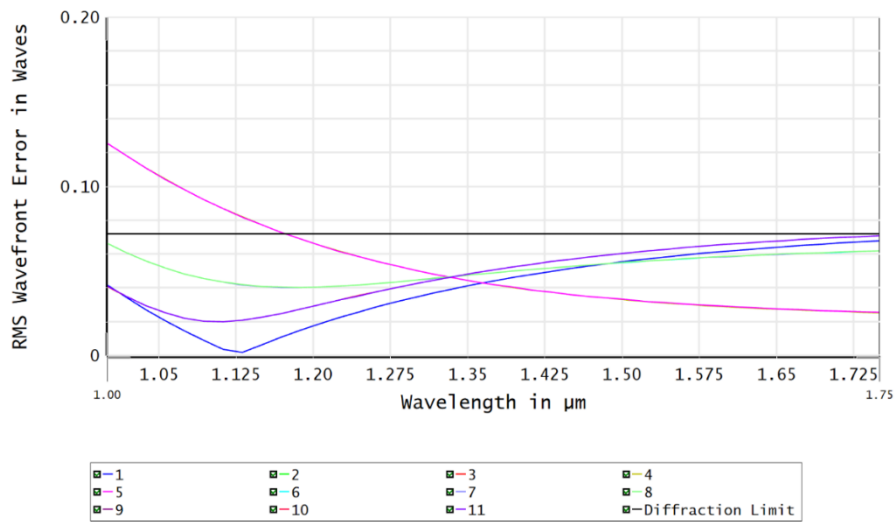


Figure 8. Nominal WFE RMS vs. wavelength in the NGS channel

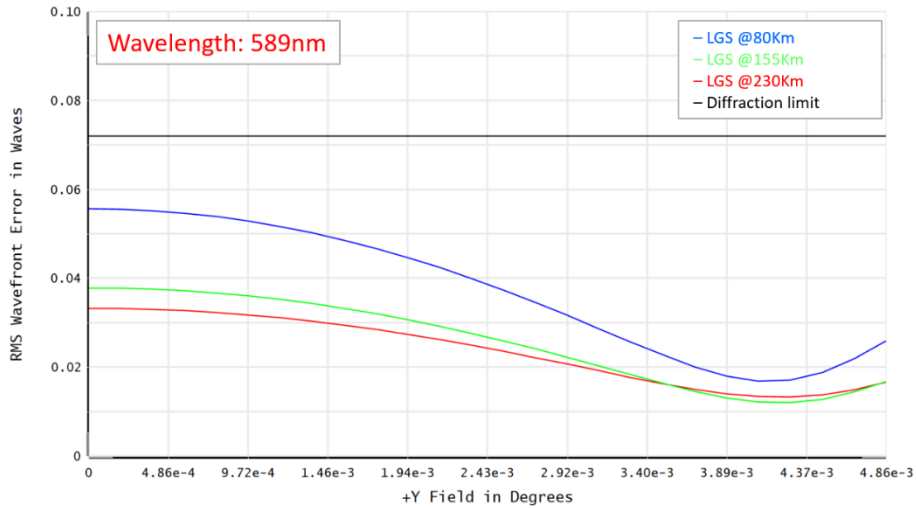


Figure 9. Nominal WFE RMS vs. field of view in the LGS channel

The use of relatively low-powered optical elements and a careful choice of glasses, together with a smart positioning of the elements along the optical train, allows to get a good correction of chromatic and geometrical aberrations and nearly zero distortion at the output focal planes with the use of a small number of optical elements and a beneficial effect on the overall throughput of the instrument. On the other hand, many optical elements are in the VIS/NIR common path, which is positive for minimization of NCPAs, but at the same time it represents a challenge for the design of high-performance coatings (both anti-reflection coatings for lenses and reflective coatings for mirrors) over the full wavelength range. A preliminary estimation of the overall throughput of the PFR optics that takes into account internal transmission of glasses, Fresnel losses and coatings, is reported in Figure 10. The figure refers only to the PFR optics excluding the contributions from telescope, sub-modules and instruments.

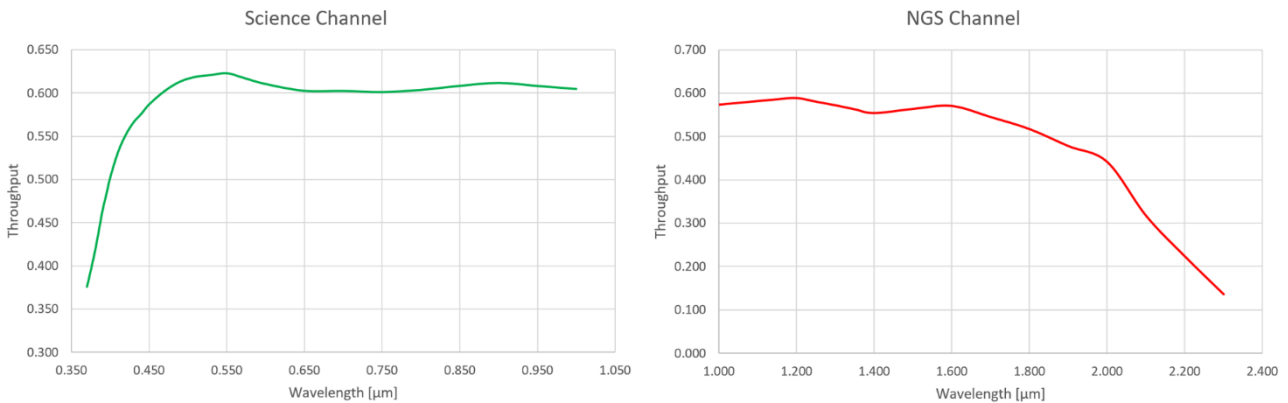


Figure 10. AOM throughput: Science (left) and NGS WFS (right) channels

The use of low-powered optical elements is also advantageous for manufacturing and alignment tolerances allowing for reasonable alignment requirements (of the order of 50-100 μ m for centering and a few arcmins for tilts for most of the elements) despite the extremely tight error budget. The tolerances have been computed by means of a sensitivity analysis including different metrics like meta-pupils image quality, average WFE RMS at the output focal planes, and maximum distortion of the NGS and SCI focal planes. At the same time, a Montecarlo simulation has shown results in agreement with the sensitivity analysis, resulting in a degradation of the image quality at the scientific focal plane of 7nm.

Concerning manufacturing tolerances, for this phase we adopted an analytic approach that takes into account the effect of the figure error of every optical surface. For this estimation, we assumed $\lambda/20$ and $\lambda/30$ tolerances on the peak-to-valley

surface quality of the lenses and of the mirrors, respectively, which results in a deterioration of the WFE of 15nm RMS. A more complete analysis is expected for the next design phase.

5. CONCLUSIONS

MAVIS, the new MCAO-assisted instrument for the VLT-UT4 has recently successfully passed the design phase A. In this paper we have presented the optical design and performance analysis of the AOM module, which is the core engine of the instrument, providing AO sensing (high-order + low-order wavefront sensors) and correction (two post-focal DMs), field de-rotation, atmospheric dispersion compensation, and enabling calibration of the system.

The proposed design is characterized by a very small residual wavefront error with nearly zero nominal distortion. The configuration is robust to alignment and manufacturing errors and is suitable to achieve the very tight requirements in terms of residual WFE set by the Strehl Ratio TLR. Moreover, the design present means to compensate for pupil motion and to compensate for defocus between the instruments and the NGS WFS sub-module. Finally, the design is modular, meaning that every sub-module can be developed and tested in most of its functionalities independently from the other parts. This is helpful to ease the interactions within the consortium and to mitigate the risk of any delay affecting one of its parts.

The current design provides three output ports: one for the imager, one for the IFU spectrograph and a third one for visiting instruments. All of this is achieved in a quite compact volume where the positioning of the sub-modules and instruments is functional for what concerns accessibility, maintenance and thermo-mechanical stability.

REFERENCES

- [1] Rigaut, F. et al., "MAVIS conceptual design," 11447-332, in these proceedings
- [2] Ellis, S. et al., "MAVIS: science case, imager, and spectrograph," 11447-285, in these proceedings
- [3] Greggio, D., Di Filippo, S., Magrin, D., Schwab, C., Viotto, V., Busoni, L., Esposito, S., Ragazzoni, R., Fusco, T., Neichel, B., Pinna, E., Rigaut, F., Arcidiacono, C., Bergomi, M., Biondi, F., Chinellato, S., Farinato, J., Marafatto, L., Portaluri, E., Santhakumari, K.K.R., and Vassallo, D., "Optical design trade-off study for the AO module of MAVIS," in AO4ELT6 proceedings (2019).
- [4] Madec, P.-Y., Kolb, J., Oberti, S., Paufigue, J., La Penna, P., Hackenberg, W., Kuntschner, H., Argomedo, J., Kiekebusch, M., Donaldson, R., Suarez, M., Arsenault, R., "Adaptive Optics Facility: control strategy and first on-sky results of the acquisition sequence", Proceedings of SPIE, 9909, 99090Z (2016).
- [5] Valentina Viotto, Guido Agapito, Davide Greggio, Cedric Plantet, Enrico Pinna, Matteo Aliverti, Carmelo Arcidiacono, Olivier Beltramo-Martin, Maria Bergomi, Marco Bonaglia, Lorenzo Busoni, Elena Carolo, Simonetta Chinellato, Jacopo Farinato, Thierry Fusco, Gaston Gausachs, Damien Gratadour, Pierre Haguenaer, Demetrio Magrin, Luca Marafatto, Benoit Neichel, Kalyan Radhakrishnan, Stefan Ströbele, Annino Vaccarella, Daniele Vassallo, Simone Esposito, Roberto Ragazzoni, David Brodrick, Francois Rigaut, "MAVIS: the adaptive optics module feasibility study", 11448-9, in these proceedings
- [6] Greggio, D., Schwab, C., Magrin, D., Di Filippo, S., Rigaut, F., Viotto, V., "Optical design of a broadband atmospheric dispersion corrector for MAVIS", 11447-263, in these proceedings
- [7] Ströbele S., La Penna P., Arsenault R., Conzelmann, R. D., Delabre B., Duchateau M., Dorn R., Fedrigo E., Hubin N., Quentin J., Jolley P., Kiekebusch M., Kirchbauer J. P., Klein B., Kolb J., Kuntschner H., Le Louarn M., Lizon J. L., Madec P.-Y., Pettazzi L., Soenke C., Tordo S., Vernet J., Muradore R., "2012: GALACSI system design and analysis," Proc. of the SPIE, 8447 (2012).
- [8] Goebel, Sean B., Hall, Donald N. B., Guyon, Olivier, Warmbier, Eric, Jacobson, Shane M., "Overview of the SAPHIRA detector for adaptive optics applications", Journal of Astronomical Telescopes, Instruments, and Systems, 4, 026001 (2018).
- [9] Gach, J.-L., Feautrier, P., Stadler, E., Clop, F., Lemarchand, S., Carmignani, T., Wanwanscappel, Y, Boutolleau, D., "C-RED One and C-RED2: SWIR high-performance cameras using Saphira e-APD and Snake InGaAs detectors", Proc. of SPIE, 10539, 1053914 (2018).
- [10] Agapito, G. et al., "MAVIS: system modelling and performance prediction," 11448-103, in these proceedings